Available online at www.sciencedirect.com
ScienceDirect
Journal of Power Sources 178 (2008) 282–290
JOURNAL OF POWER SOURCES
www.elsevier.com/locate/jpowsour

Improved oxidation resistance of a nanocrystalline chromite-coated ferritic stainless steel

Zigui Lu [a,b], Jiahong Zhu [a,*], Ye Pan [a], Naijuan Wu [b], Alex Ignatiev [b]

[a] *Department of Mechanical Engineering, Tennessee Technological University, TN 38505, USA*
[b] *Texas Center for Advanced Materials, University of Houston, TX 77204, USA*

Received 30 October 2007; accepted 29 November 2007
Available online 18 January 2008

Abstract

An economical dip coating process was developed to synthesize uniform, crack-free, and adherent thin nanocrystalline $LaCrO_3$ films on a ferritic stainless steel substrate for the solid oxide fuel cell interconnect applications. $LaCrO_3$ perovskite phase was formed after annealing in air at 800 °C for 1 h for both the $LaCrO_3$ and La_2O_3 precursors. The effectiveness of the coating in improving the oxidation resistance of the alloy was demonstrated by both isothermal and cyclic oxidation tests. The $LaCrO_3$ coatings were found to cause a pronounced reduction in oxidation rate of the alloy, especially with low La-content precursors. The area-specific resistance of the oxide scales formed on the bare and coated alloy substrates was also evaluated and discussed.

Keywords: Solid oxide fuel cell; Interconnect; Dip coating; Oxidation resistance

1. Introduction

As the operating temperature of solid oxide fuel cell (SOFC) reduces to below 800 °C, metallic alloys can be used as the interconnect material. Metallic interconnect offers many advantages over ceramic interconnect, such as high thermal and electrical conductivity, good ductility, and low cost of raw materials and fabrication, etc. Cr_2O_3-forming alloys, such as Ebrite, Crofer-22APU and Haynes 230 are promising candidates for the interconnect applications because these alloys form a thin, protective layer of Cr_2O_3 scale on the alloy surface upon thermal exposure. Ferritic Cr_2O_3-forming alloys are especially attractive because of their low cost and close match in coefficient of thermal expansion (CTE) with other fuel cell components. One major concern with these alloys is their long-term stability and compatibility with other fuel cell components as a result of continuous Cr_2O_3 scale growth [1–3] and Cr migration to the cathode side through gaseous Cr species [4]. While the Cr_2O_3 scale growth increases the area-specific resistance (ASR) of the oxide scale, the migration of Cr species to the cathode side can cause the degradation of the cathode performance during cell operation [5–8].

To mitigate these problems, surface modification or surface coating on the Cr-containing ferritic alloy substrate is an attractive approach. The surface coating, if dense and crack-free, is expected to act as a seal to the volatile Cr species and provide oxidation protection for the metallic substrate. Some of the major criteria for coating selection are low Cr evaporation rate, adequate electrical conductivity, close CTE match with the substrate, and high thermal stability at SOFC operating environments. Several perovskite materials, such as doped $LaMnO_3$, $LaCoO_3$, $LaFeO_3$, and $LaCrO_3$ are potential choices. $LaCrO_3$-based coating attracts more attention because of its high stability in both reducing and oxidizing atmospheres, reasonable electrical conductivity, proper CTE match with the metallic substrate, and lower Cr evaporation rate than Cr_2O_3.

There are many techniques to deposit coatings on metallic substrates, such as sputtering [9], electron-beam physical vapor deposition (EB-PVD), laser ablation [10], chemical vapor deposition (CVD), screen-printing [11,12], plasma spraying [13], and wet chemical techniques [14–16]. Among these techniques, both PVD and CVD have the disadvantages of relatively low deposition rates, expensive equipment, high

* Corresponding author. Tel.: +1 931 372 3186; fax: +1 931 372 6340.
E-mail address: jzhu@tntech.edu (J. Zhu).

0378-7753/$ – see front matter © 2007 Elsevier B.V. All rights reserved.
doi:10.1016/j.jpowsour.2007.11.105

deposition temperature, and/or involvement of corrosive gases in some cases. Screen-printing is economical and can produce coatings with thickness larger than 10 μm, but the coatings are usually porous. The sol–gel route, which is usually for thin film (less than 1 μm) deposition, offers the advantages of good homogeneity and composition control, low sintering temperature, low cost, and ease of scale-up, etc.

Although many attempts have been made to deposit protective coatings on metallic substrates by various methods [10–17], very few papers focused on the effect of the coatings on mass change of the alloys and ASR change of the oxide scale over long periods of oxidation at high temperatures [9,18]. In this paper, an economical dip coating process was used to synthesize thin, dense, and uniform coatings of $LaCrO_3$ on Ebrite substrates from both $LaCrO_3$ and La_2O_3 precursors. It is found that the deposited La_2O_3 layer reacts with the thermally grown Cr_2O_3 to form $LaCrO_3$ upon thermal exposure [15,19,20]. The effectiveness of these coatings was evaluated by both isothermal and cyclic oxidation tests at 900 °C in air. The surface structures and morphologies of the coated and bare samples before and after oxidation tests were examined with a number of techniques. The ASR of the coated samples after long-term oxidation was also evaluated.

2. Experimental procedures

2.1. Coating synthesis

Two series of La_2O_3 and $LaCrO_3$ precursor solutions for dip coating were prepared via the following procedure: $La(NO_3)_3$ (99.999% pure, Alfa Aesar, Ward Hill, MA) or $La(NO_3)_3$ with $Cr(NO_3)_3$ (99% pure, Sigma–Aldrich, Milwaukee, WI) were dissolved in distilled water, citric acid (99.5+% pure, Alfa Aesar, Ward Hill, MA) was then added as a chelating agent. The solutions were stirred overnight until homogeneous solutions were achieved. These solutions were heated on a hot plate at about 80 °C to expel water and achieve a desired concentration. Concentrations from 0.05 to 0.25 mol L^{-1} (M) were used in both cases. A surface tension relieving agent was added into the solution to increase surface wettability. A commercial iron-based alloy Ebrite with the composition of Fe–26Cr–1Mo–0.02Mn–0.24Si (all in wt.%, as provided by the industrial supplier) was selected as the substrate for this study. The as-received sheet was first cut into a 10 mm × 10 mm × 0.5 mm square plate, followed by grinding and polishing to a 0.3 μm Al_2O_3 finish. The polished samples were then cleansed ultrasonically in acetone for 5 min prior to dip coating.

The dip coating process was performed with a KSV single vessel dip coater (KSV Instrumental Ltd., Monroe, CT), with a linear immersing and pulling speed of 1 mm s^{-1}. The coated specimens were dried at 80 °C, followed by calcination at 600 °C for 10 min in the furnace. To build up the thickness of the coating, the whole coating process was repeated several times with intermediate drying and calcinations. Finally, the coated specimens were annealed at 800 °C for 1 h in air.

2.2. Oxidation tests

Short-term isothermal oxidation tests of the $LaCrO_3$-coated specimens (10 coating runs) were carried out in a Cahn thermobalance with a linear heating rate of 75 °C min^{-1} to determine the oxidation kinetics. The samples were oxidized at 900 °C for 50 h in flowing air with a volumetric flow rate of 45 mL min^{-1}. The mass change of the sample was recorded as a function of time.

Long-term cyclic oxidation tests of coated Ebrites (10 coating runs) were carried out in stagnant air using a box furnace. Each cycle consists of heating to 900 °C in 45 min, holding at 900 °C for 100 h, and furnace cooling to 100 °C; the total number of cycles is 10 for each sample, with a cumulative exposure time of 1000 h. The mass change of the samples was recorded for each cycle after the samples were cooled down to room temperature in a desiccator to avoid moisture pick-up.

2.3. Microstructural characterization

The surface structure and morphology of the bare and coated samples before and after oxidation were analyzed using X-ray diffraction (XRD) and scanning electron microscopy (SEM). The thickness of the as-deposited coating or thermally grown oxide scale was estimated by SEM cross-sectional observation before and after oxidation.

2.4. Electrical resistance of the oxide scales

The ASR of the oxide scale formed on the bare and coated specimens after oxidation was measured as a function of temperature in air by using a 2-point, 4-wire approach [21]. The two oxidized surfaces of the sample were covered with Pt paste and cured at 850 °C for 30 min. Two Pt meshes each with two Pt leads were fixed on top of the Pt paste to collect current. A constant current of 10 mA was passed through two Pt leads on each side and the voltage between the other two leads was recorded. The ASR was calculated according to Ohm's law, ASR = $SV/2I$, where S, I, and V are the Pt covered surface area of the sample, the applied current, and the measured voltage drop, respectively. A factor of 2 is used to account for the fact that the voltage drop was measured across two oxide scales formed on both sides of the sample surfaces.

3. Results and discussion

3.1. Thin film formation

Fig. 1 shows the surface morphologies of the $LaCrO_3$ coatings on the Ebrite substrate after annealing in air at 800 °C for 1 h. A uniform, smooth, and adherent coating was achieved for the whole surface area in all cases. However, the coatings from $LaCrO_3$ and La_2O_3 precursors exhibited different surface morphological features. For the coatings prepared from low concentration $LaCrO_3$ precursor (e.g. 0.05 M precursor), as shown in Fig. 1(a), the coating consisted of many fine grains of less than 100 nm in diameter. The coating was very thin since the

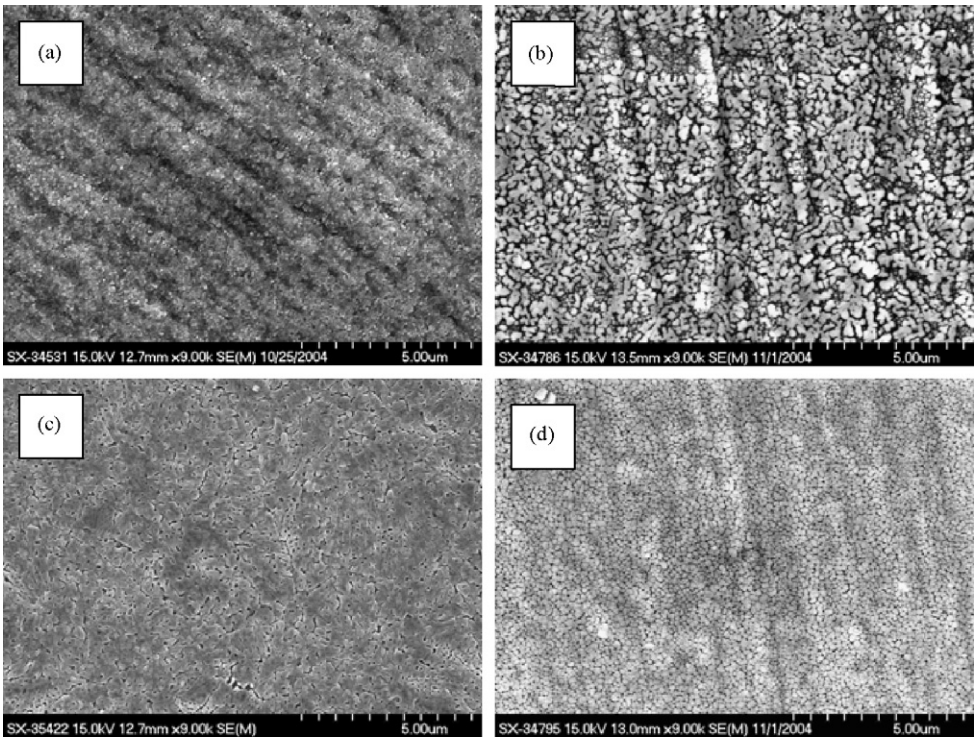

Fig. 1. SEM surface morphologies of $LaCrO_3$- and La_2O_3-coated Ebrite samples (8 coating runs) after annealing at 800 °C for 1 h: $LaCrO_3$ coating with a precursor concentration of (a) 0.05 M and (c) 0.25 M, and La_2O_3 coating with a precursor concentration of (b) 0.05 M and (d) 0.25 M.

grinding marks on the substrate can be clearly seen in the SEM picture. This conclusion was further confirmed by the low intensity of the perovskite peaks compared to that of the substrate in the XRD results. However, no cracks or pinholes can be found in the coatings. For the coating from high $LaCrO_3$ concentration precursor (0.25 M), which was shown in Fig. 1(c), the grains of $LaCrO_3$ coating were connected to each other to form a network of fine and roundish dendrite structures, with grain boundary and a few pinholes present in the coating. As the precursor concentration increased, both the thickness and grain size of the coating increased. Perovskite phase was formed without any preferred orientation in the coating, as implied by XRD results (Fig. 5). The surface morphology of the $LaCrO_3$ coating from 0.25 M precursor was very similar to that of the $LaCrO_3$ coatings fabricated through RF sputtering by Orlovskaya et al. [22] and spin coating by Belogovsky et al. [18]. Compared to the coating by Orlovskaya et al., the coating from sol–gel process was more uniform and smooth over a larger scale.

The $LaCrO_3$ coatings from the La_2O_3 precursor consisted of uniformly self-assembled grains, especially for the 0.25 M precursor. The grain size of $LaCrO_3$ coating decreased with precursor concentration, from about 300 to 100 nm in diameter as the concentration of the precursor increased from 0.05 to 0.25 M. The coatings were also relatively thin as the grinding marks were still visible in the SEM pictures. The thickness of the coating increased with coating runs. Fig. 2 shows the XRD patterns of the $LaCrO_3$ coatings from different concentration of La_2O_3 precursors with different numbers of coating runs. The intensity of $LaCrO_3$ peaks increased with the La_2O_3 precursor concentration and the number of coating runs. It is interesting to note that the relative intensity of the perovskite peaks was different for the precursors with different concentrations. Precursors with a high concentration (e.g. 0.25 M) led to the formation of perovskite phase with strong peaks of (1 1 0) and (2 2 0), while the low concentration precursor (e.g. 0.05 M) resulted in perovskite structure with a strong peak of (2 0 0). XRD results indicate that Cr_2O_3 was also formed on the surface of the substrate in all

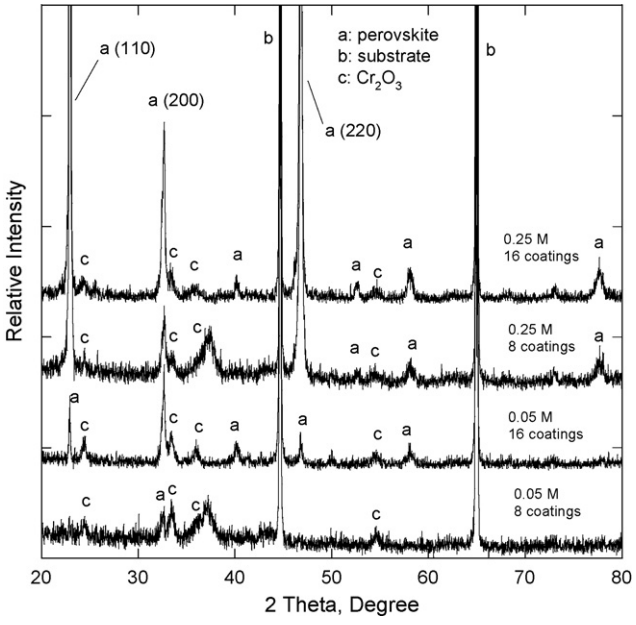

Fig. 2. XRD patterns of La_2O_3-coated Ebrite samples with different coating runs and precursor concentrations.

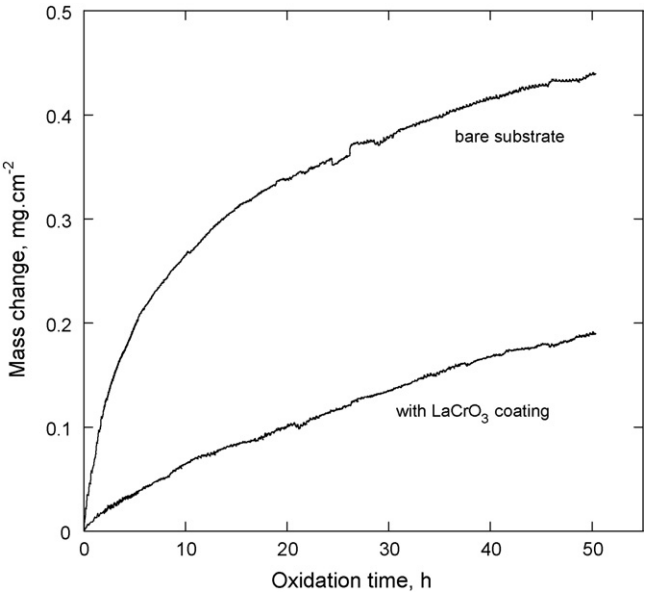

Fig. 3. Isothermal oxidation kinetics of the bare and $LaCrO_3$-coated Ebrite samples at 900 °C for 50 h.

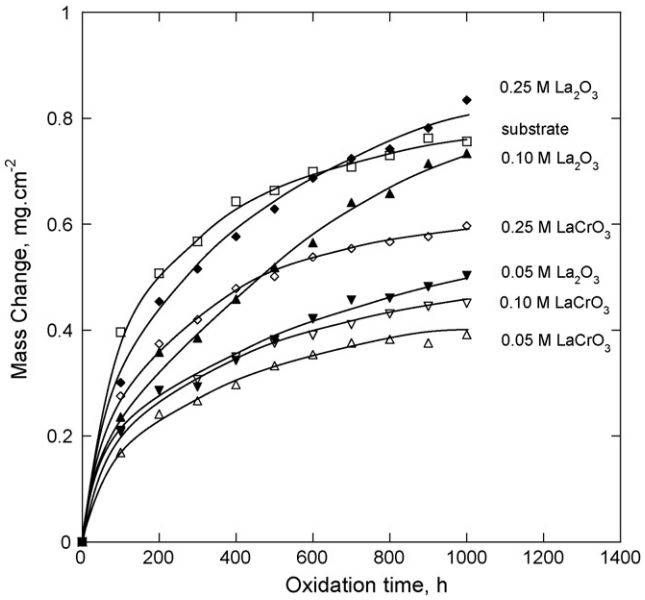

Fig. 4. Mass changes of $LaCrO_3$- and La_2O_3-coated Ebrite during cyclic oxidation test (ten 100-h cycles) at 900 °C in air.

La_2O_3 precursor coated samples after annealing at 800 °C for 1 h.

3.2. Oxidation behaviors of uncoated and coated samples

Fig. 3 plots the mass changes of the bare substrate and $LaCrO_3$-coated substrate at 900 °C in air for 50 h, which was carried out with a Cahn thermo-balance. A near parabolic behavior was observed for both bare and coated samples. According to the parabolic law:

$$\left(\frac{\Delta W}{A}\right)^2 = k_o t \quad (1)$$

where ΔW is the weight change, A the surface area of the sample, k_o the parabolic rate constant, and t is the oxidation time. From Fig. 3, the rate constants k_o for both bare and coated samples were calculated to be 1.07×10^{-12} and 1.99×10^{-13} $g^2\,cm^{-4}\,s^{-1}$, respectively. The parabolic rate constant of the bare Ebrite was very close to that reported by Huang et al. (9.8×10^{-13} $g^2\,cm^{-4}\,s^{-1}$) [2] and Belogovsky et al. [18]. The parabolic rate constant of $LaCrO_3$ coated samples was 5 times lower than that of bare substrate, indicating the effectiveness of the coating in reducing the oxidation rate of the Ebrite substrate at the early stage of oxidation.

The mass change curves of the bare and coated Ebrite cyclically oxidized at 900 °C in air are given in Fig. 4. The samples were oxidized for 10 cycles, with each cycle of 100 h and the cumulative oxidation time of 1000 h. All the coated samples exhibited smaller mass gains than the bare Ebrite substrate initially; the bare substrate had an initial weight change of 0.40 mg cm^{-2} for the first 100 h, while the $LaCrO_3$-coated specimen from 0.05 M $LaCrO_3$ precursor only had a weight change of 0.17 mg cm^{-2}, less than half of that for the bare substrate. It is clearly shown that the coating protected the substrate effectively from oxidation at high temperatures. For each type of precursor, the mass gain increased with the precursor concentration. Overall, the La_2O_3 precursor-coated specimens had larger weight gains than the $LaCrO_3$ precursor-coated specimens with a similar precursor concentration, possibly because the La_2O_3 precursor-coated specimen would consume the Cr_2O_3 subscale to form $LaCrO_3$. As the oxidation continued, the oxidation curves could be divided into two categories. The first category with low precursor concentrations of $LaCrO_3$ (both 0.05 and 0.10 M) and La_2O_3 (0.05 M) exhibited a slower mass increase, while the second category with high concentrations of $LaCrO_3$ (0.25 M) and La_2O_3 (both 0.10 and 0.25 M) registered a faster mass increase. No spallation of the coating was observed during oxidation tests in all cases.

The phase structures of the coatings before and after cyclic oxidation tests were characterized by XRD. Because the phase structures of the coatings from the same types of precursors were very similar, only the results for the coating from the 0.25 M $LaCrO_3$ and La_2O_3 precursors were given here, as shown in Figs. 5 and 6, respectively. After the oxidation test, Cr_2O_3 was the major oxidation product formed on the Ebrite substrate without coating, with a small amount of the spinel phase, as shown in Figs. 5 and 6. For the $LaCrO_3$-coated specimens (Fig. 5), Cr_2O_3 was also formed between the coating and substrate. However, the peaks of the perovskite coating retained even after 1000-h oxidation at 900 °C, although the intensity of the $LaCrO_3$ peaks became weaker with oxidation time. Other than the perovskite and Cr_2O_3 peaks, spinel phase also appeared as a major oxidation product on the coated specimens. The La_2O_3 precursor-coated specimens after the oxidation tests exhibited very similar XRD results (Fig. 6) as the $LaCrO_3$ precursor-coated specimens, with Cr_2O_3 and spinel formed on the coated samples while the $LaCrO_3$ perovskite phase was still retained.

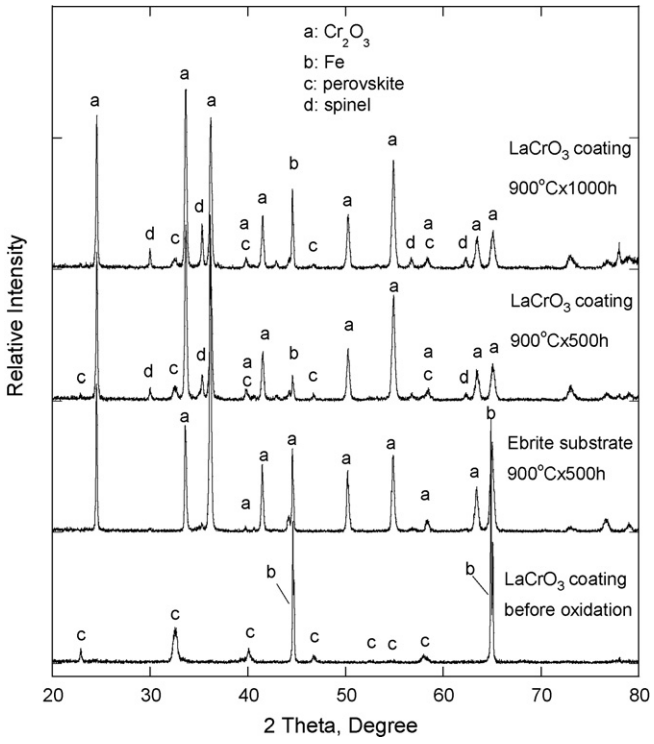

Fig. 5. XRD patterns of $LaCrO_3$-coated Ebrite before and after cyclic oxidation test at 900 °C in air for different times.

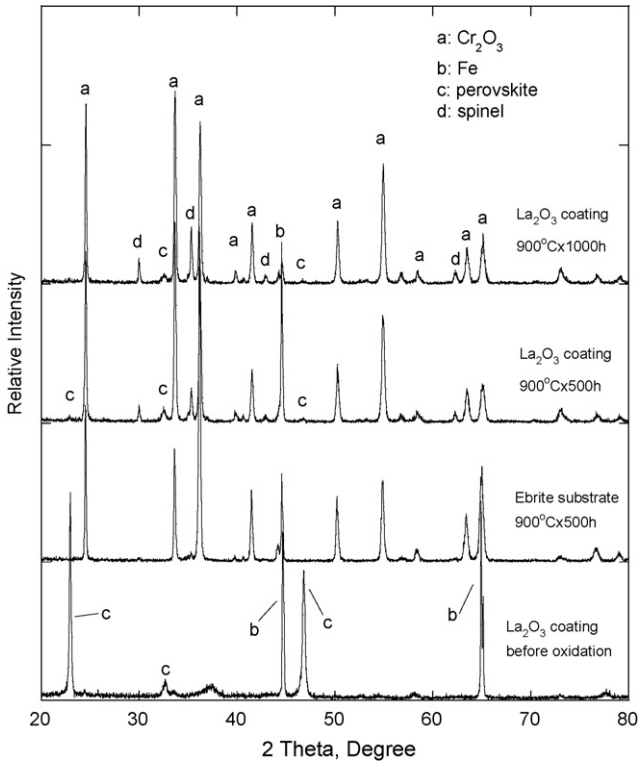

Fig. 6. XRD patterns of La_2O_3-coated Ebrite before and after cyclic oxidation test at 900 °C in air for different times.

Fig. 7 shows the surface morphology and cross-section of the oxide scale formed on bare Ebrite substrate after oxidation at 900 °C for 1000 h. The oxide scale was composed of small Cr_2O_3 nodules with about 2–5 μm in diameter. The thickness of the Cr_2O_3 scale after oxidation at 900 °C for 1000 h was about 5–6 μm. Some porosity was observed at the interface between the oxide scale and substrate.

The surface morphologies of the $LaCrO_3$-coated Ebrite after the oxidation test were different from that of substrate. The coating surface from low concentration $LaCrO_3$ precursor (0.05 M) was composed of very fine particles with isolated large particles on top, see Fig. 8(a). EDS results indicated that the large particles were pure Cr_2O_3 which were embedded in a layer of $(Fe,Cr)_3O_4$ spinel. Cross-section of this sample [Fig. 9(a)] indicated that there were two layers of oxides formed, the top one with $(Fe,Cr)_3O_4$ spinel structure and the bottom one Cr_2O_3. No distinctive $LaCrO_3$ layer could be observed because this layer was too thin and was partially dissolved into the oxide scale after the oxidation test. The thickness of the two oxide layers of spinel and Cr_2O_3 was about 0.5 and 2–3 μm, respectively. The rest of the coatings, including the coating from 0.25 M $LaCrO_3$ precursor and all of the La_2O_3 precursors, exhibited another feature, as shown in Fig. 8(b)–(d). The coatings were composed of large, convoluted, "worm-like" grains, which were twisted with each other. These elongated grains had a diameter of about 10–20 μm. SEM image with high magnification of these grains revealed that these grains were made of small particles of 500 nm in diameter. The thickness of the oxide scale for all coated samples was similar, about 4–6 μm. The thickness of the oxide scale is consistent with the mass gain after cyclic oxidation tests for all the samples.

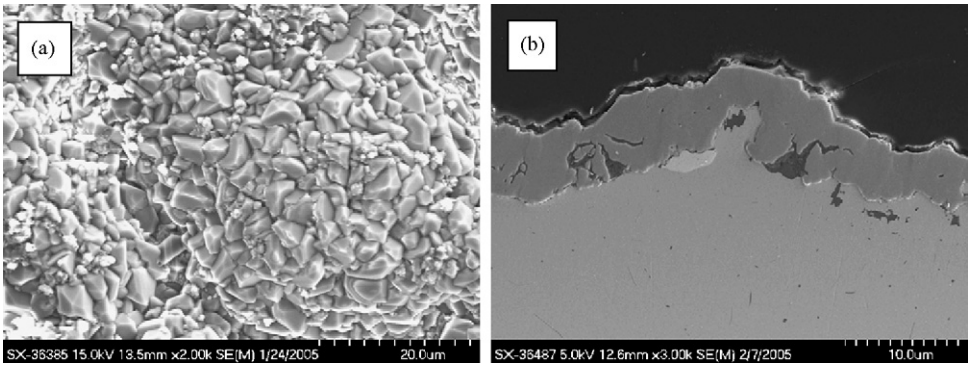

Fig. 7. Surface morphology and cross-section of the Ebrite substrate after the oxidation test at 900 °C for 1000 h: (a) surface and (b) cross-section.

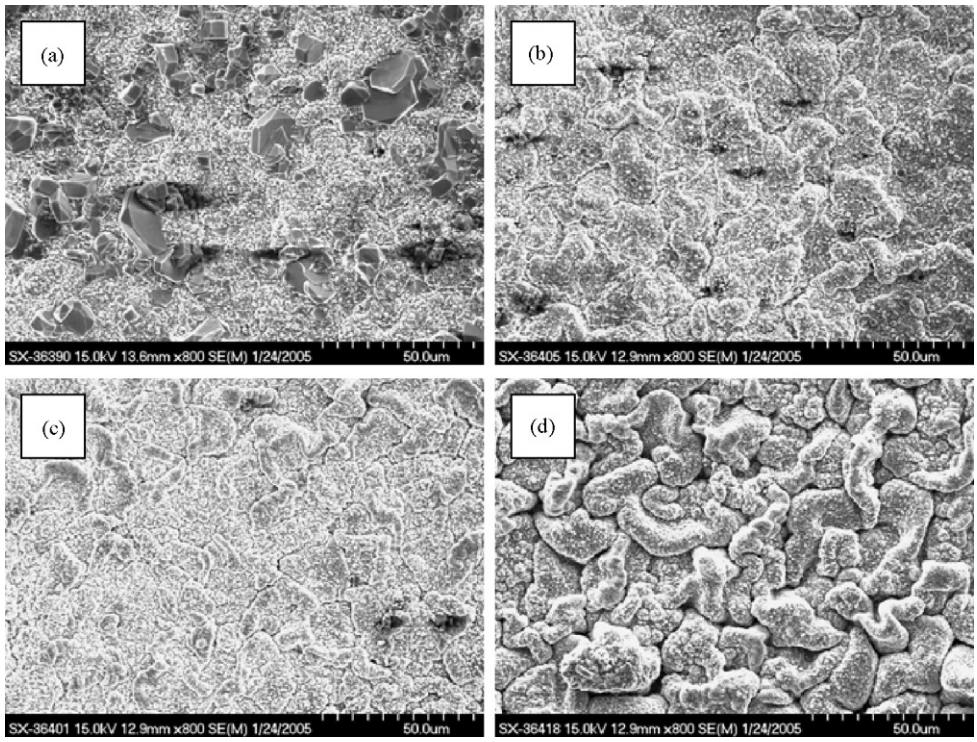

Fig. 8. Surface morphologies of the $LaCrO_3$- and La_2O_3-coated Ebrite samples after the oxidation test at 900 °C for 1000 h: $LaCrO_3$ coating with a precursor concentration of (a) 0.05 M and (c) 0.25 M, and La_2O_3 coating with a precursor concentration of (b) 0.05 M and (d) 0.25 M.

The ultimate goal of forming the $LaCrO_3$ coating on the Ebrite substrate is to improve the oxidation resistance of the substrate and at the same time, to reduce Cr migration from the oxide scale to the cathode side. Both the isothermal (Fig. 3) and cyclic (Fig. 4) oxidation test results clearly demonstrated that the coating was effective in reducing the oxidation rate of the substrate. However, the oxidation behaviors varied for the different coatings, which is probably due to the different structures of the coatings resulting from the specific formation mechanisms. For the $LaCrO_3$ precursor, the perovskite phase can directly be formed from the precursor since the precursor contains both La and Cr; for the La_2O_3 precursor, La_2O_3 will be formed right after film synthesis, then the La_2O_3 coating will consume the thermal-grown Cr_2O_3 scale to form the $LaCrO_3$ perovskite during subsequent annealing. XRD results of the La_2O_3 precursor-coated samples show no peaks from La_2O_3; instead, $LaCrO_3$ and Cr_2O_3 peaks appeared after annealing at 800 °C for 1 h (Fig. 2). For $LaCrO_3$-coated samples, only $LaCrO_3$ peaks were detected in the XRD patterns (Fig. 5).

The Ebrite substrate had a larger initial mass gain than the coated samples for the first 100-h oxidation. The mass increase rate then slowed down after 400-h oxidation. The mass gain of La_2O_3 precursor-coated samples from high concentration precursor (e.g. 0.25 M) had a lower initial mass gain than the bare substrate. Nevertheless, its mass gain increased more rapidly than that of the bare substrate. After 600-h oxidation, the 0.25 M La_2O_3 precursor-coated sample even had larger mass gain than the bare substrate. An unambiguous explanation is still unavailable at this stage. Clearly, the evaporation of Cr at 900 °C could not fully account for more rapid weight increase of the 0.25 M

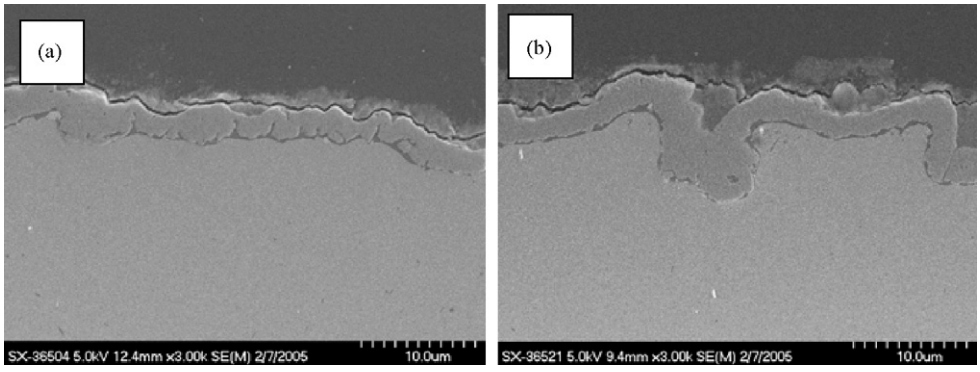

Fig. 9. Cross-section of the coated Ebrite samples after the oxidation test at 900 °C for 1000 h: (a) $LaCrO_3$ coating with a precursor concentration of 0.05 M and (b) La_2O_3 coating with a precursor concentration of 0.05 M.

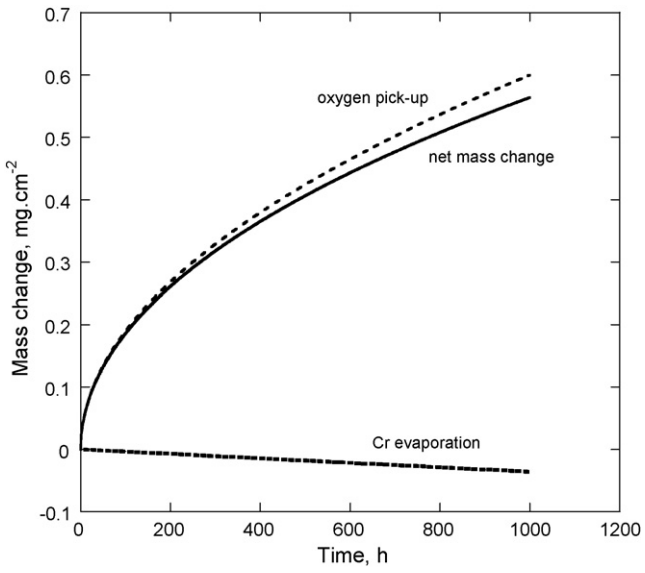

Fig. 10. Simulated curves of mass change due to oxidation and Cr evaporation, assuming k_o and k_e to be 10^{-12} and 2.6×10^{-11} g cm^{-2} s^{-1}, respectively.

La_2O_3 precursor-coated samples, as the following discussions demonstrated this point clearly.

Due to the Cr evaporation at high temperatures, the net mass change of the sample is a combination of oxidation and Cr evaporation. Oxidation of the sample will pick up oxygen from the atmosphere, while Cr evaporation will cause mass loss of the sample. The mass changes due to oxidation and Cr evaporation is proportional to the square root of time and time, respectively. Therefore, the weight change of the sample can be expressed as

$$\frac{\Delta W}{A} = \sqrt{k_o t} - k_e t \quad (2)$$

ΔW, A and k_o have the same meanings as in Eq. (1); k_e is the evaporation rate constant of Cr species. k_o has the value at the order of 10^{-12} g^2 cm^{-4} s^{-1} for Ebrite substrate from our results, as well as the results by Huang et al. and Belogovsky et al. [2,18]. For pure Cr_2O_3-forming alloys such as Ducralloy, k_e has the reported value of 1.32×10^{-11} and 4.92×10^{-11} g cm^{-2} s^{-1} at 850 and 950 °C, respectively [23]. Therefore, k_e is approximated to be 2.6×10^{-11} g cm^{-2} s^{-1} at 900 °C, assuming k_e is exponential to the reciprocal of temperature. Fig. 10 shows the simulated curves of mass change over time with the consideration of both oxidation and Cr evaporation. It can be clearly seen that Cr evaporation at this temperature will not make significant contribution to the net mass change. After 1000 h at 900 °C, the weight loss due to Cr evaporation is about only 6% of mass gain due to oxidation. Therefore, Cr evaporation is not the major reason for the faster weight increase of La_2O_3 precursor-coated samples than the Ebrite substrate, even though the deposition or formation of $LaCrO_3$ thin film on the substrate is expected to suppress the Cr evaporation because the Cr volatility of $LaCrO_3$ is more than 3 orders of magnitude lower than that of Cr_2O_3 [24].

One possible explanation for the rapid oxidation of coated samples from high concentration precursors is related to the so-called reactive element effect (REE) [25]. It was discovered long time ago that minor additions of rare earth elements in Al_2O_3- or Cr_2O_3-forming alloys greatly improved the oxidation resistance and the scale-alloy adhesion. Although the mechanism of REE is still not well understood, its commercial application and importance has been widely recognized and investigated [26–28]. The amount of reactive element needed in the alloy to produce the REE is typically between 0.1 and 0.2 at.%. However, amounts over 1 at.% generally lead to a deterioration in the scale adhesion and fast oxidation. Our cyclic oxidation results indicates that for the same type of precursor, the mass gain increased with the precursor concentration. Therefore, the lower precursor concentration leads to lower reactive element content in the surface region of the alloys, which is probably more close to the desired concentration. Further increase in the precursor concentration seems detrimental to the oxidation resistance, because of the over-doping of the reactive elements. This conclusion is further supported by the fact that the La_2O_3 precursor-coated samples from 0.05 M precursor had very similar mass gains with the $LaCrO_3$ precursor-coated ones from 0.10 M precursor up to 500 h oxidation because they essentially had the same La content in the precursor.

3.3. ASR of the oxidized samples

The ASR that reflects both the electrical conductivity and the thickness of the oxide scale has been adopted to evaluate the electrical properties of the oxidized samples. It is generally assumed that the resistivity of the metallic substrate is negligible compared to that of the oxide scale. The measured ASR, therefore, includes only that of the oxide scale itself and its interfaces with the alloy and electrodes. Since in the current 2-probe 4-wire method, a low constant current is used, the interfacial polarization is also negligible [2]. Fig. 11 presents the

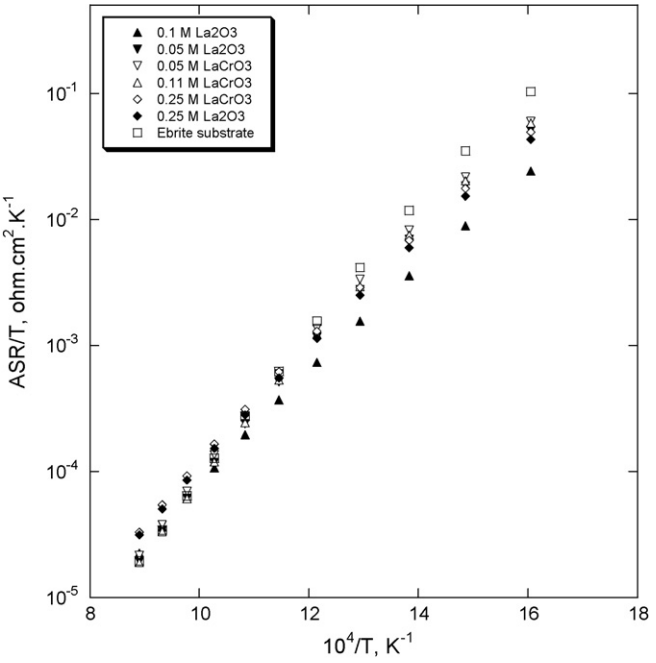

Fig. 11. ASR of the bare and coated Ebrite samples after the cyclic oxidation test at 900 °C in air for 1000 h.

ASR/T of the bare and coated Ebrite samples versus 10^4/T after the oxidation test at 900 °C for 1000 h. It is intriguing that although the coated samples from low La concentration precursors had thinner oxide scales than the bare substrate and high La concentration precursor-coated samples, all the ASRs were very similar, especially at high temperatures. However, the ASR of bare substrate increased more quickly than that of the coated ones. Therefore, at low temperatures, oxidized Ebrite substrate possessed the higher ASR than the coated Ebrite samples. Among the coated samples, the one from 0.1 M La_2O_3 precursor had the lowest ASR after the oxidation test. From Fig. 11, the apparent activation energies, E_a, for the ASR were obtained by fitting to an Arrhenius expression and plotted in Fig. 12:

$$\frac{\mathrm{ASR}}{T} = A_0 \exp\left(\frac{E_a}{RT}\right) \quad (3)$$

where A_0 is a constant, R the gas constant, and T is the absolute temperature. The activation energies of the uncoated and coated samples decreased with La concentration of the precursors, as Fig. 12 illustrates. The uncoated Ebrite has activation energy of 1.06 eV, while the activation energies of the coated samples decreased from 0.98 to 0.85 eV as the La concentration of the precursor increased from 0.05 to 0.50 M. Huang et al. [14] reported the activation energies of 0.90 and 0.71 eV for uncoated and Y-coated Ebrite, which are very similar to our results. According to Huang et al., the apparent activation energy contains contribution from the electrode/scale interface (ΔH_i), the oxide scale (ΔH_m), and the metal/scale interface (ΔH_j). In our case, because we used the same electrode material (Pt) in all electrical conductivity measurements, ΔH_i should remain approximately same, so the difference must result from either ΔH_m or ΔH_j or both. Therefore, the reduction of activation energy either comes from the change of the oxide scale formed on the substrate or the improved oxide scale/alloy interface adhesion. It is still unclear why the sample from a higher La-content precursor has a reduced activation energy at this stage.Conclusions

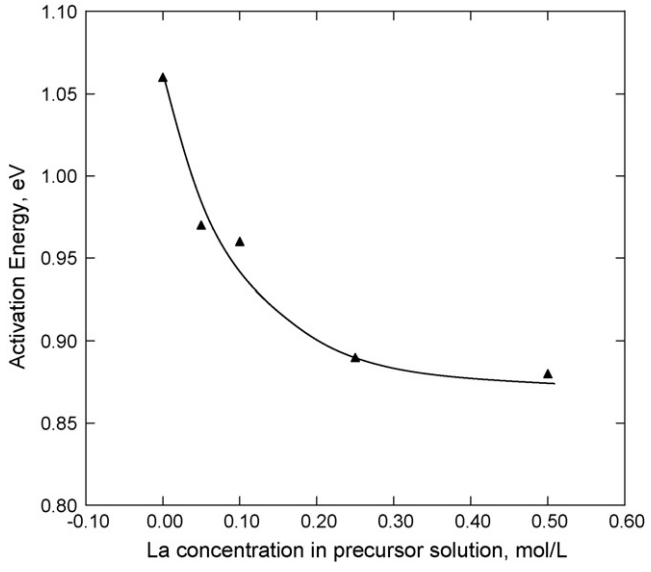

Fig. 12. Activation energies for the oxidized samples from the precursors with various La concentrations.

A thin, dense, crack-free, and adherent nanocrystalline $LaCrO_3$ coating was successfully deposited on Ebrite substrate by dip coating. Different concentrations of the precursor solutions led to different surface morphologies of the coating after final annealing at 800 °C for 1 h. The coating with 0.05 M $LaCrO_3$ precursor reduced the weight gain of the Ebrite substrate at 900 °C from 0.40 to 0.17 mg cm^{-2} for 100 h and from 0.76 to 0.39 mg cm^{-2} for 1000 h. No spallation was observed in all cases. The thickness of the thermally formed oxide scale of uncoated Ebrite substrate was about 6 μm, while the thickness for the coated samples from low La concentration precursors reduced to about 3 μm after oxidation at 900 °C for 1000 h. The $LaCrO_3$ phase was still retained in the coating after oxidation at 900 °C for 1000 h. ASR results revealed that the $LaCrO_3$ coating also reduced the ASR of the oxide scale formed during oxidation, especially at low temperatures. Reactive element effect might be used to explain the observed oxidation rate for the coated alloys.

Acknowledgements

This investigation was financially supported by the National Science Foundation under Grant # DMR-0238113. Part of this work was also supported by the DOE SECA Core Technology Program (Award No. DE-FC26-04NT42223) and by the Assistant Secretary for Energy Efficiency and Renewable Energy, Office of FreedomCAR and Vehicle Technologies, as part of the High Temperature Materials Laboratory User Program, Oak Ridge National Laboratory, managed by UT-Battelle, LLC for DOE under contract number DE-AC05-00OR22725.

References

[1] W.Z. Zhu, S.C. Deevi, Mater. Sci. Eng. A 348 (2003) 227.
[2] K. Huang, P.Y. Hou, J.B. Goodenough, Solid State Ionics 129 (2000) 237.
[3] S.P.S. Badwal, R. Deller, K. Foger, Y. Ramprakash, J.P. Zhang, Solid State Ionics 99 (1997) 297.
[4] M.C. Tucker, H. Korokawa, C.P. Jacobson, L.C. DeJonghe, S.J. Visco, J. Power Sources 160 (2006) 130.
[5] Y.S. Taniguchi, M. Kadowaki, H. Kawamura, T. Yasuo, Y. Akiyama, Y. Miyake, J. Power Sources 55 (1995) 73.
[6] S.P. Jiang, J.G. Love, L. Apateanu, Solid State Ionics 160 (2003) 15.
[7] Y. Matsuzaki, I. Yasuda, Solid State Ionics 132 (2000) 271.
[8] S.C. Paulson, V.I. Birss, J. Electrochem. Soc. 151 (2001) A1961.
[9] Z. Yang, G. Xia, G.D. Maupin, J.W. Stevenson, J. Electrochem. Soc. 153 (2006) A1852.
[10] A. Kajimura, H. Sasaki, S. Otoshi, M. Suzuki, C. Kurusu, N. Sugiura, M. Ippommatsu, Solid State Ionics 82 (1995) 107.
[11] K. Przybylski, J. Prazuch, T. Brylewski, T. Maruyama, Proceedings of the 14th International Corrosion Congress, October 1999, p. 122.
[12] T. Brylewski, K. Przybylski, J. Morgiel, Mater. Chem. Phys. 81 (2003) 434.
[13] L.J.H. Kuo, S.D. Vora, S.C. Singhal, J. Am. Ceram. Soc. 80 (1997) 589.
[14] K. Huang, P.Y. Hou, J.B. Goodenough, Mater. Res. Bull. 36 (2001) 81.
[15] J.H. Zhu, Y. Zhang, A. Basu, Z.G. Lu, M. Parathaman, D.F. Lee, E.A. Payzant, Surf. Coat. Technol. 177–178 (2004) 65.
[16] W. Qu, J. Li, D.G. Ivey, J. Power Sources 138 (2004) 162.
[17] X. Chen, P.Y. Hou, C.P. Jacobson, S.J. Visco, L.C. De Jonghe, Solid State Ionics 176 (2005) 425.

[18] I. Belogovsky, X. Zhou, H. Kurokawa, P. Hou, S. Visco, H.U. Anderson, J. Electrochem. Soc. 154 (2007) B976.
[19] N. Oishi, T. Namikawa, Y. Yamazaki, Surf. Coat. Technol. 132 (2000) 58.
[20] S. Lingderoth, Surf. Coat. Technol. 80 (1996) 185.
[21] S.J. Geng, J.H. Zhu, Z.G. Lu, Solid State Ionics 177 (2006) 559.
[22] N. Orlovskaya, A. Coratolo, C. Johnson, R. Gemmen, J. Am. Ceram. Soc. 87 (2004) 1981.
[23] C. Gindorf, L. Singheiser, K. Hilpert, Steel Res. 72 (2001) 528.
[24] K. Hilpert, D. Das, M. Miller, D.H. Peck, R. Weiß, J. Electrochem. Soc. 143 (1996) 3642.
[25] P.Y. Hou, J. Stringer, Mater. Sci. Eng. A 202 (1995) 1.
[26] J. Stringer, B.A. Wilcox, R.I. Jaffee, Oxid. Met. 5 (1972) 11.
[27] G.M. Ecer, R.B. Singh, G.H. Meier, Oxid. Met. 18 (1982) 55.
[28] P. Papaiacovou, R.J. Hussey, D.F. Mitchell, M.J. Graham, Oxid. Met. 33 (1990) 19.